Asociación Argentina
de Mecánica Computacional

Mecánica Computacional Vol XXX, págs. 2609-2626 (artículo completo)
Oscar Möller, Javier W. Signorelli, Mario A. Storti (Eds.)
Rosario, Argentina, 1-4 Noviembre 2011

NUMERICAL INVESTIGATION OF THE WIND ACTION OVER LOW-RISE BUILDINGS USING LARGE EDDY SIMULATION AND A SINTHESIZED TURBULENCE GENERATOR

Alexandre Luis Braun[a] **and Armando Miguel Awruch**[b]

[a]*Department of Civil Engineering, Federal University of Rio Grande do Sul (DECIV/UFRGS), Av. Osvaldo Aranha 99, Porto Alegre, Brazil, allbraun@ig.com.br*
http://www6.ufrgs.br/engcivil/deciv/

[b]*Graduate Program in Civil Engineering, Federal University of Rio Grande do Sul (PPGEC/UFRGS), Av. Osvaldo Aranha, 99, Porto Alegre, Brazil, amawruch@ufrgs.br*
http://www6.ufrgs.br/engcivil/ppgec/

Keywords: Computational Wind Engineering (CWE), Large Eddy Simulation (LES), Synthesized Turbulence, Finite Element Method (FEM), Building Aerodynamics.

Abstract. A numerical model using Computational Wind Engineering (CWE) techniques is employed in this work to investigate the wind action over low-rise buildings. The increase observed in the global temperature of the earth during the last decades, which is mainly originated by climatic changes induced by the greenhouse effect, has lead to the development of cyclones and tornadoes over areas located in the southern region of Brazil. These climatic phenomena have produced important damages to low-rise buildings like houses, warehouses, silos and gymnasiums. In conjunction with experimental tests employing wind tunnels and recommendations proposed by the Brazilian standard (NBR-6123: Forças Devidas ao Vento em Edificações), numerical simulation has been considered lately as an important alternative to evaluate the wind action on buildings and to predict possible failures. A numerical model based on the Finite Element Method is adopted here to simulate the action of wind flows over low-rise civil structures, where the influence of turbulent fluctuations on the incident stream is also considered by using a numerical method to generate synthesized fluctuations over the inlet boundary conditions. Important information such as aerodynamic coefficients and flow fields around the buildings are obtained. Examples related to buildings usually subjected to structural damages during the incidence of strong winds are analyzed and results are compared with experimental predictions obtained from wind tunnel tests.

1 INTRODUCTION

The increase observed in the global temperature of the earth, which is manly induced by the well known greenhouse effect, has lead to the incidence of meteorological phenomena such as tornadoes, cyclones and hurricanes on regions where this kind of occurrence was rarely verified before. It is well known today that the formation of tropical cyclones is directly associated to elevated ocean temperatures. According to CPTEC/INPE (*Centro de Previsão de Tempo e Estudos Climáticos / Instituto Nacional de Pesquisas Espaciais; visit http://www.cptec.inpe.br/*), a federal bureau belonging to the Brazilian Ministry of Science and Technology, tropical cyclones and hurricanes are usually observed when a low pressure center, which is traveling over tropical oceans, meets waters with temperatures above 26°C. Cyclones are characterized by wind speeds up to 120 km/h, whereas hurricanes present wind speeds in the range between 200 and 300 km/h. On the other hand, the occurrence of tornadoes is related to strong storms. Tornadoes are also characterized by climatologic events of short duration (a few minutes), covering short distances (500 to 1500 m) and with wind speeds usually exceeding 200 km/h.

The southern region of Atlantic Ocean did not present conditions to develop extreme meteorological phenomena until the occurrence of Hurricane Catarina (see Fig. 1) in March 2004, which covered some areas of two southern Brazilian states, more precisely the coast of Santa Catarina and the northeast region of Rio Grande do Sul. The phenomenon was formed on March 23, being observed during the following four days. An extratropical cyclone was originated above the Atlantic Ocean first, reaching then the coast with wind speeds exceeding 180 km/h and bringing devastation and death to large areas. Unfortunately, some studies performed during the last years have demonstrated that the oceans are tending to warm, including South Atlantic, and whether the temperature of the seas increases continuously with the global warming, more regions of South Atlantic will present temperatures above 26ºC during the most part of the year, which is a basic condition to develop cyclones and hurricanes.

Figure 1 – Satellite images of Hurricane Catarina (CPTEC/INPE and NASA).

In the Brazilian standard code on determination of wind loads over civil structures (NBR 6123 - Forças Devidas ao Vento em Edificações), a fundamental parameter to evaluate the dynamic pressure induced by the wind flow is referred to as basic speed, which is obtained from a map of isolines showing the distribution of wind speeds throughout the Brazilian territory. That basic speed represents the wind speed related to a wind gust with three seconds length measured at 10 m above a plane and open field, which can only be exceeded once during 50 years. When the southern region of Brazil is observed, one can verify that the basic speed presents maximum values ranging from 45 to 50 m/s, which is equivalent to speeds of 162 and 180 km/h, respectively. Considering the wind speeds associated to cyclones and hurricanes, it is concluded that a careful evaluation of loads induced by the wind action

during those events must be carried out, especially for low-rise buildings such as houses, warehouses, silos and gymnasiums, which may present structural characteristics more susceptible to damages originated by aerodynamic loads. Low-rise buildings are considered as rigid and do not exhibit significant dynamic effects. Damages are usually induced by differences observed between internal and external pressure distributions over building walls and roofs.

For specific situations such as those related to buildings with unusual shapes and unusual wind characteristics, the Brazilian standard code NBR 6123 indicates additional studies to be performed in a wind tunnel in order to evaluate the aerodynamic loads accurately. Nevertheless, owing to important improvements observed in the fields of computer technology and numerical modeling, simulations performed with CFD techniques have demonstrated that numerical simulation can be considered today as a feasible alternative to experimental analysis in wind tunnels (see, for instance, Braun and Awruch, 2005; Braun and Awruch, 2008; Braun and Awruch, 2009). In this sense, the present work is devoted to simulate the wind action on low-rise buildings using CWE (computational wind engineering), where special CFD techniques are adopted in order to reproduce wind flows numerically.

Although other alternatives may be taken into account to analyze turbulent flows numerically, it is observed that Large Eddy Simulation (LES) have been widely employed in the field of CWE (see Tamura, 2008). Despite the large computational resources required, LES provides excellent results when compared to experimental predictions and other numerical models. However, natural wind flows can only be reproduced adequately if a numerical algorithm to generate turbulence fluctuations over the incidence flow is incorporated into the numerical model, since LES alone is not able to produce instantaneous turbulent inlet boundary conditions. Several techniques have been presented during the last decades, where precursor simulations and synthetic generators are the most common. Considering that precursor simulations require important storage resources and expensive processing efforts, it is observed that late researches have been directed to methods of generation using synthetic turbulence. Synthetic turbulence generators can be much more economic and faster when compared to other methods. Moreover, they are able to satisfy any prescribed spectrum and the divergence-free condition without additional numerical procedures (see, for instance, Davidson, 2007; Huang et al., 2010).

In the numerical model presented here an explicit two-step Taylor-Galerkin scheme is utilized for the discretization of the flow governing equations considering incompressible flows and Newtonian fluids, where the pseudo-compressibility hypothesis is assumed in order to obtain pressure fields explicitly (see Braun, 2007). The FEM is employed for spatial approximations over the flow field, where eight-node hexahedral elements with one-point quadrature and hourglass control are adopted. Turbulence is analyzed using LES with the dynamic sub-grid model (see Smagorinsky, 1963; Germano et al., 1991; Lilly, 1992) and a synthetic turbulence generator is utilized to obtain inflow turbulence boundary conditions satisfying spatial correlation and other turbulence characteristics. Some numerical simulations involving low-rise building models are carried out and results obtained with the present formulation are compared to experimental predictions obtained from wind tunnel analyses.

2 THE FLOW GOVERNING EQUATIONS

Wind engineering flows are usually simulated considering the Navier-stokes equations and the mass conservation equation under isothermal conditions, where turbulence modeling must be taken into account to avoid excessive computational efforts. In order to circumvent drawbacks observed in the continuity equation owing to the incompressible flow assumption,

the pseudo-compressibility hypothesis may be adopted (Chorin, 1967). In this sense, the governing equations employed in the present work to reproduce wind flow fields may be expressed as follows:

$$\frac{\partial v_\mathrm{i}}{\partial t} + v_\mathrm{j}\frac{\partial v_\mathrm{i}}{\partial x_\mathrm{j}} = \frac{1}{\rho}\frac{\partial \sigma_\mathrm{ij}}{\partial x_\mathrm{j}} \qquad (\mathrm{i, j} = 1,2,3) \tag{1}$$

$$\frac{\partial p}{\partial t} + v_\mathrm{j}\frac{\partial p}{\partial x_\mathrm{j}} + \rho c^2\frac{\partial v_\mathrm{j}}{\partial x_\mathrm{j}} = 0 \qquad (\mathrm{j} = 1,2,3) \tag{2}$$

where v_i denotes components of the velocity vector according to the direction of the Cartesian axes x_i, p represents the thermodynamic pressure, ρ is the fluid density and c is the sound speed in the flow field. In addition, body forces are neglected. The system of governing equations introduced above is valid for a spatial domain Ω_f and a time interval T, where $t \in [0,T]$.

The Cauchy stress tensor σ_ij may be decomposed into thermodynamic pressure and viscous parts as follows:

$$\sigma_\mathrm{ij} = -p\delta_\mathrm{ij} + \tau_\mathrm{ij} \qquad (\mathrm{i, j} = 1,2,3) \tag{3}$$

where δ_ij are components of the Kroenecker's delta ($\delta_\mathrm{ij} = 1$ for $i = j$; $\delta_\mathrm{ij} = 1$ for $i \neq j$) and τ_ij are components of the viscous stress tensor, which is expressed according to the Newtonian constitutive formulation and the Stokes hypothesis (see White, 2005), that is:

$$\tau_\mathrm{ij} = \left(\mu + \mu_\mathrm{t}\right)\left(\frac{\partial v_\mathrm{i}}{\partial x_\mathrm{j}} + \frac{\partial v_\mathrm{j}}{\partial x_\mathrm{i}}\right) + \lambda\frac{\partial v_\mathrm{k}}{\partial x_\mathrm{k}}\delta_\mathrm{ij} \qquad (\mathrm{i, j, k} = 1,2,3) \tag{4}$$

where μ and λ are the kinematic and volumetric viscosities of the fluid, respectively. Notice that the eddy viscosity is introduced in order to indicate turbulence modeling, which is performed here considering the LES methodology with the dynamic sub-grid model (Lilly, 1992), where two filtering procedures are applied over the flow governing equations taking into account a filter based on the finite element mesh and a second filter defined with a larger size. After the filtering procedures, the flow governing equations are described in terms of filtered variables, which are associated to the large scales of turbulence. Turbulence scales smaller than the grid resolution must be represented using a turbulence model, where an expression to determine the eddy viscosity is obtained. In the present work, the eddy viscosity at element level is defined according to the dynamic model as follows:

$$\mu_\mathrm{t} = \rho C\left(x_\mathrm{i}, t\right)\overline{\Delta}^2\left|S_\mathrm{ij}\right| \qquad (\mathrm{i, j} = 1,2,3) \tag{5}$$

where S_ij are components of the strain rate tensor and $\overline{\Delta}$ defines the characteristic dimension of the first filter, which is obtained from $\overline{\Delta} = \left(\Omega_\mathrm{E}\right)^{1/3}$, considering that Ω_E is the volume of element E. The dynamic coefficient $C(x_\mathrm{i},t)$ is determined automatically according to instantaneous conditions of the flow, where (x_i,t) denotes space and time dependencies. Further details on the numerical procedures adopted in this work to obtain the eddy viscosity may be found in Braun (2007) e Braun and Awruch (2009).

In order to obtain the numerical solution of the flow governing equations, initial conditions for the flow variables must be defined at $t = 0$. Moreover, boundary conditions must be also imposed over the flow variables as follows:

$$v_{\mathrm{i}} = v_{\mathrm{i}}^{*} \quad \text{on } \Gamma_{\mathrm{v}} \tag{6}$$

$$p = p^{*} \quad \text{on } \Gamma_{\mathrm{p}} \tag{7}$$

$$\left[-p\delta_{\mathrm{ij}} + \mu\left(\frac{\partial v_{\mathrm{i}}}{\partial x_{\mathrm{j}}} + \frac{\partial v_{\mathrm{j}}}{\partial x_{\mathrm{i}}} \right) + \lambda \frac{\partial v_{\mathrm{k}}}{\partial x_{\mathrm{k}}} \delta_{\mathrm{ij}} \right] n_{\mathrm{j}} = t_{\mathrm{i}}^{*} \quad \text{on } \Gamma_{\sigma} \tag{8}$$

where v_{i}^{*}, p^{*} and t_{i}^{*} represent prescribed values related to velocity, pressure and traction, respectively. These prescribed values are imposed on Γ_{v}, Γ_{p} and Γ_{σ}, respectively, which correspond to the boundaries of the flow spatial domain Ω_{f}. In Eq. (8), n_{j} denotes components of the unit normal vector at a specific point belonging to Γ_{σ}.

When turbulence fluctuations are considered in the incidence flow, inflow boundary conditions are modified to include a turbulent velocity field generated synthetically (see, for instance, Davidson, 2007; Huang et al., 2010), which may be obtained using *N* random Fourier modes as follows:

$$v_i'(x_j) = 2\sum_{n=1}^{N} \hat{v}^n \cos(\kappa_j^n x_j + \psi^n)\, \sigma_i^n \tag{9}$$

where v_i' are components of the fluctuating velocity vector given according to the Cartesian directions x_{i}, which are defined at a specific point with coordinates x_{j}, and $\hat{v}^n$ and ψ^n are amplitude and phase associated to Fourier mode *n*, respectively. The wave number vector κ_j^n and the velocity unit vector σ_i^n, which also indicates the direction of Fourier mode *n*, are orthogonal in the spatial domain for each wave number *n*, since the unit vector σ_i^n must satisfy continuity, that is $\sigma_i^n \kappa_i^n = 0$. The direction of σ_i^n in the plane $\xi_1^n - \xi_2^n$ is randomically obtained considering the angle α^{n}. Furthermore, σ_3^n must be parallel to ξ_3^n, indicating that σ_3^n is chosen to be parallel to κ_i^n (see Fig. 2). The angles φ^{n} and θ^{n} and the phase φ^{n} are also obtained randomically.

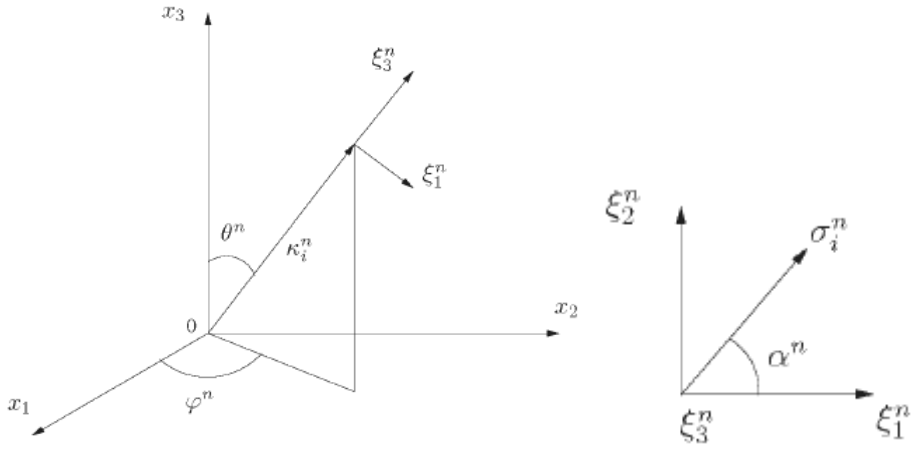

Figure 2 – Defining the wave number direction (Davidson, 2007).

The amplitude $\hat{v}^n$ for each mode is obtained considering a modified von Kármán spectrum as follows:

$$\hat{v}^n = \sqrt{E\left(\left|\kappa_j^n\right|\right)\Delta\kappa} \tag{10}$$

where:

$$E(\kappa) = 1.453\frac{v_{rms}^2}{\kappa_e}\frac{(\kappa/\kappa_e)^4}{\left[1+(\kappa/\kappa_e)^2\right]^{17/6}}e^{\left[-2(\kappa/\kappa_\eta)^2\right]} \tag{11}$$

with:

$$\kappa = \left(\kappa_i\kappa_i\right)^{1/2} \tag{12}$$

$$\kappa_\eta = \varepsilon^{1/4}\nu^{-3/4} \tag{13}$$

$$\kappa_e = 1.453\frac{9\pi}{55L_t} \tag{14}$$

where v_{rms} represents the standard deviation of the streamwise velocity, ε is the rate of energy dissipation, ν is the kinematic viscosity and L_t is the turbulence length scale. Figure 3 shows the modified von Kármán spectrum, where $\kappa_1 = \kappa_e/p$ is defined as the smallest wave number and $\Delta\kappa = (\kappa_{max} - \kappa_1)/N$ is the equally spaced wave number interval. The factor p is chosen to be larger than one in order to make the largest scales larger than those corresponding to κ_e. The highest wave number is defined considering the mesh resolution, that is $\kappa_{max} = 2\pi/(2\Delta)$, where Δ is the grid spacing.

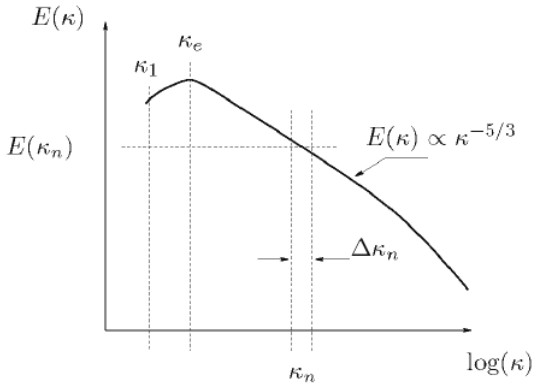

Figure 3 – Modified von Kármán spectrum (Davidson, 2007).

In order to obtain a fluctuating velocity field with time correlation, since the fluctuations generated with the formulation presented above are independent of each other, a time filter must be employed over the response computed with Eq. (9). An asymmetric time filter may be adopted as follows (see Klein et al., 2003):

$$(\overline{v}_i')^n = a(\overline{v}_i')^{n-1} + b(v_i')^n \tag{15}$$

with:

$$a = e^{-\Delta t/\tau}; \qquad b = (1-a^2)^{1/2} \tag{16}$$

where n and n-1 denote the current and previous time steps, respectively, and τ is the turbulence time scale, which is usually approximated as:

$$\tau = \frac{L_t}{v_{rms}} \tag{17}$$

Further details on the numerical model adopted here to generate turbulence fluctuations are found in Davidson (2007).

The inlet boundary conditions corresponding to Eq. (6) are then rewritten as follows:

$$v_{\mathrm{i}} = V_i + \overline{v}_i' \quad \text{on } \Gamma_{\mathrm{v}}^{\mathrm{inlet}} \tag{18}$$

where V_{i} are components of the time average velocity vector according to the Cartesian directions x_{i} and $\Gamma_{\mathrm{v}}^{\mathrm{inlet}}$ denotes the boundary surface corresponding to the entrance of the computational domain.

3 THE NUMERICAL MODEL

The solution fields for the flow governing equations are obtained in this work employing a numerical model based on the explicit two-step Taylor-Galerkin scheme (Kawahara and Hirano, 1983; Braun, 2007). In this model, temporal derivatives are first approximated by Taylor series expansions up to second order terms and the Bubnov-Galerkin weighted residual method is then applied to the discretized equations into the context of the FEM (Zienkiewicz et al., 2005). Spatial dicretization is performed considering eight-node hexahedral elements with one-point point quadrature, where a stabilization scheme is adopted in order to avoid the incidence of spurious modes due to hourglass instability. For additional information on the numerical model adopted in this work see Braun (2007).

The algorithm for solution of the flow governing equations may be summarized as follows:

(I) Solve the momentum equations to obtain a first approximation for the velocity field at the intermediate point of the time step, that is $\overline{v}_i^{n+1/2}$:

$$\overline{v}_i^{n+1/2} = v_i^n + \frac{\Delta t}{2}\left\{-v_j\frac{\partial v_i}{\partial x_j} - \frac{1}{\rho}\frac{\partial p}{\partial x_j}\delta_{ij} + \frac{\partial}{\partial x_j}\left[\frac{\mu+\mu_t}{\rho}\left(\frac{\partial v_i}{\partial x_j}+\frac{\partial v_j}{\partial x_i}\right)+\frac{\lambda}{\rho}\frac{\partial v_k}{\partial x_k}\delta_{ij}\right]+\left(\frac{\Delta t}{4}v_j v_k\right)\frac{\partial^2 v_i}{\partial x_j x_k}\right\}^n$$

where μ_{t} must be previously obtained from Eq. (5).

(II) Impose the boundary conditions specified by Eqs. (6) and (8) (or Eqs. 18 and 8) on the velocity field $\overline{v}_i^{n+1/2}$.

(III) Solve the mass conservation equation to obtain the pressure field at the intermediate point of the time step, that is $p^{n+1/2}$:

$$p^{n+1/2} = p^n + \frac{\Delta t}{2}\left\{\left[-v_j\frac{\partial p}{\partial x_j} - \rho c^2\frac{\partial v_j}{\partial x_j}\right]+\left(\frac{\Delta t}{4}v_i v_j\right)\frac{\partial^2 p}{\partial x_j \partial x_i}\right\}^n$$

(IV) Impose the boundary condition specified by Eq. (7) on the pressure field $p^{n+1/2}$.

(V) Determine the pressure increment:

$$\Delta p^{n+1/2} = p^{n+1/2} - p^n$$

(VI) Determine the corrected velocity field using the pressure increment obtained above, that is $v_i^{n+1/2}$:

$$v_i^{n+1/2} = \overline{v}_i^{n+1/2} - \frac{1}{\rho}\frac{\Delta t^2}{8}\frac{\partial \Delta p^{n+1/2}}{\partial x_i}$$

(VII) Impose the boundary conditions specified by Eqs. (6) and (8) (or Eqs. 18 and 8) on the corrected velocity field $v_i^{n+1/2}$.

(VIII) Update the velocity field using $v_i^{n+1} = v_i^n + \Delta v_i^{n+1/2}$, where:

$$\Delta v_i^{n+1/2} = \Delta t\left\{-r_j\frac{\partial v_i}{\partial x_j} - \frac{1}{\rho}\frac{\partial p}{\partial x_j}\delta_{ij} + \frac{\partial}{\partial x_j}\left[\frac{\mu+\mu_t}{\rho}\left(\frac{\partial v_i}{\partial x_j}+\frac{\partial v_j}{\partial x_i}\right)+\frac{\lambda}{\rho}\frac{\partial v_k}{\partial x_k}\delta_{ij}\right]\right\}^{n+1/2}$$

(IX) Impose the boundary conditions specified by Eqs. (6) e (8) (or Eqs. 18 and 8) on the updated velocity field v_i^{n+1}.

(X) Update the pressure field using $p^{n+1} = p^n + \Delta p^{n+1/2}$, where:

$$\Delta p^{n+1/2} = \Delta t\left\{-r_j\frac{\partial p}{\partial x_j} - \rho c^2\left(\frac{\partial v_j}{\partial x_j}\right)\right\}^{n+1/2}$$

(XI) Impose the boundary condition specified by Eq. (7) on the updated pressure field p^{n+1}.

(XII) Return to step I and proceed with the next time step until the time march ends.

Since the numerical model utilized in this work presents an explicit nature, the time step adopted in the time discretization must be carefully determined in order to maintain the numerical stability. The time step is limited to a specific value related to physical aspects associated to the sound propagation through the matter, which is obtained according to the well known Courant condition:

$$\Delta t = \alpha\frac{\Delta x_{\mathrm{E}}}{\mathrm{V}_{\mathrm{E}} + c} \tag{19}$$

where Δx_{E} is the characteristic dimension of element *E*, V_{E} the characteristic velocity associated to element *E*, *c* is the sound speed in the physical medium and α is a safety coefficient, which is always smaller than unity. In the present work, the time step is defined taking into account the smaller time step obtained from Eq. (19), which is usually related to the smaller element of the finite element mesh.

4 NUMERICAL EVALUATION OF AERODYNAMIC COEFFICIENTS

Aerodynamic forces are developed over the body surface of structures immersed in a fluid stream. These forces are usually obtained by integration of pressures and shear stresses developed on the fluid-structure interface owing to the flow action. The components of the aerodynamic forces in the along-flow and cross-flow directions are referred to as drag and lift, respectively. In the present work, the aerodynamic force coefficients are evaluated using the formulae presented below:

$$C_{Fx} = \frac{\sum_{i=1}^{NNI} (F_x)^i}{1/2\,\rho V_\infty^2 HW}; \quad C_{Fy} = \frac{\sum_{i=1}^{NNI} (F_y)^i}{1/2\,\rho V_\infty^2 HL}; \quad C_{Fz} = \frac{\sum_{i=1}^{NNI} (F_z)^i}{1/2\,\rho V_\infty^2 WL} \tag{20}$$

where *i* denotes a nodal point located on the fluid-structure interface, V_∞ is the flow reference speed, NNI is the number of fluid nodal points on the body surface and L, W and H are characteristic dimensions related to length, width and height of the immersed body, respectively. The aerodynamic forces F_x, F_y and F_z at a nodal point *i* are obtained by numerical integration of Eq. (8) over the body surface. For further details on the numerical scheme adopted in this work to calculate forces induced by the flow, readers are addressed to Braun (2007).

The pressure coefficient for a point located on the fluid-structure interface can be calculated using the following expression:

$$C_p^i = \frac{p_i - p_0}{\frac{1}{2}\rho V_\infty^2} \tag{21}$$

where p_0 is a reference pressure, which is usually associated to undisturbed regions of the flow, and p_i may be considered as instantaneous or time average values referring to the pressure at nodal points *i* belonging to the fluid-structure interface.

5 NUMERICAL APPLICATIONS

In the present section, results obtained with the numerical model proposed in this work are presented. Aerodynamic analyses were carried out considering low-rise building models utilized previously in experimental studies performed in the LAC wind tunnel (Laboratório de Aerodinâmica das Construções – LAC/PPGEC/UFRGS). In addition, the wind action over a circular silo with conical roof is also investigated numerically. Experimental predictions obtained by other authors are taken into account when comparisons with the results obtained in the present work are performed. The building models analyzed here were idealized without openings over the building walls, where communication between external and internal environments is not allowed. The wind characteristics adopted in the numerical analyses carried out here are in agreement with wind characteristics observed during extreme climatological events.

5.1 Aerodynamic analysis of low-rise building models

Analyses are carried out here in order to determine pressure distributions over the external surface of low-rise building models. Two building models are considered in the present study, which present rectangular shapes with cylindrical and pitched roofs. Information related to model identification and the respective geometrical parameters are found in Table 1. In accordance with the wind characteristics adopted in the wind tunnel tests, a uniform distribution for the wind speed along the height is adopted in both simulations. Turbulence on the incident stream is considered with 11% intensity and a longitudinal length scale proportional to the respective building widths (*b*), which are supposed to be the most important scales for the correct evaluation of pressure loads. Physical and time dicretization constants adopted by the numerical model during the present investigations are presented in Table 2, where a Reynolds number of $3x10^5$ can be identified for both models.

Identification	a x b x h [m]
MOD 1	16 x 8 x 2
MOD 2	16 x 4 x 2

Table 1 – Identification of the low-rise building models investigated in this work and their respective geometrical characteristics.

Proprieties	Models	
	MOD 1	MOD 2
Mass density (ρ) [Kg/m^3]	1.25	1.25
Dynamic viscosity (μ) [Ns/m^2]	$8x10^{-4}$	$5.8x10^{-4}$
Volumetric viscosity (λ) [Ns/m^2]	0.0	0.0
Sound speed (c) [m/s]	170	170
Reference velocity V [m/s]	30	30
Reference dimension D [m]	8	5.8
Time step Δt [s]	$1.2x10^{-4}$	$1.2x10^{-4}$

Table 2 – Physical and time constants adopted in the numerical analysis of low-rise building models.

The geometrical characteristics of the building models and the corresponding finite element meshes may be visualized in Fig. 4, where the number of elements and nodes are also indicated. The roof slope for the building model with pitched roof is 15° and the height and the radius of the cylindrical roof correspond to 0.80 m and 2.90 m, respectively. Nonslip boundary conditions are considered on the building surfaces as well as on the ground level. The inflow boundary conditions are imposed considering a steady wind speed with uniform distribution along the height, over which a fluctuating signal must be added employing the turbulence generator proposed in this work. Outflow boundary conditions with constant pressure distribution and flow symmetry on the side and top walls of the computational domain are also prescribed. In both the cases studied here the building longitudinal direction is aligned to the flow direction.

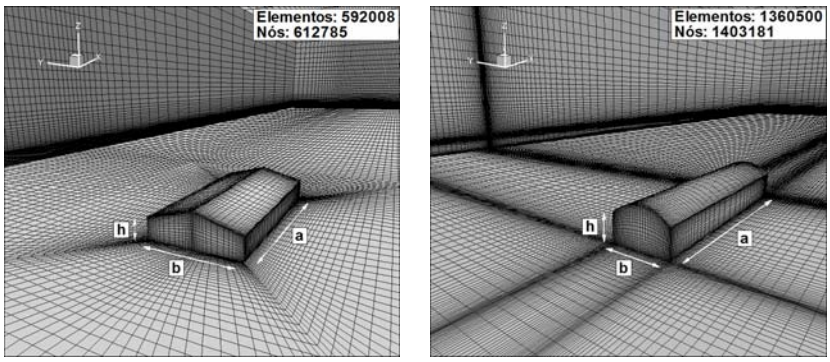

(a) (b)

Figure 4 – Finite element meshes and geometrical characteristics utilized in the numerical analysis of low-rise building models: (a) MOD 1; (b) MOD 2.

Time average pressure distributions over the center line of the roof surface are presented in Fig. 5, where results obtained in the present simulations are compared with predictions obtained from experimental studies carried out in the LAC/PPGEC/UFRGS wind tunnel. In

addition, time average pressure distributions on the front and back walls are also presented considering the intermediate longitudinal section of the buildings analyzed here. Unfortunately, experimental results other than those referring to the pressure distribution over the center line of the roof surface of the buildings were not reported. One can observe that the numerical model was able to reproduce the general aspects related to the pressure behavior on the roof surface, especially for zones far from the separation region, which corresponds to the zone where the most relevant differences between numerical and experimental predictions are identified. It is important to notice that pressures on the separation areas are very difficult to be reproduced numerically as well as experimentally, since significant pressure gradients are usually observed in those regions.

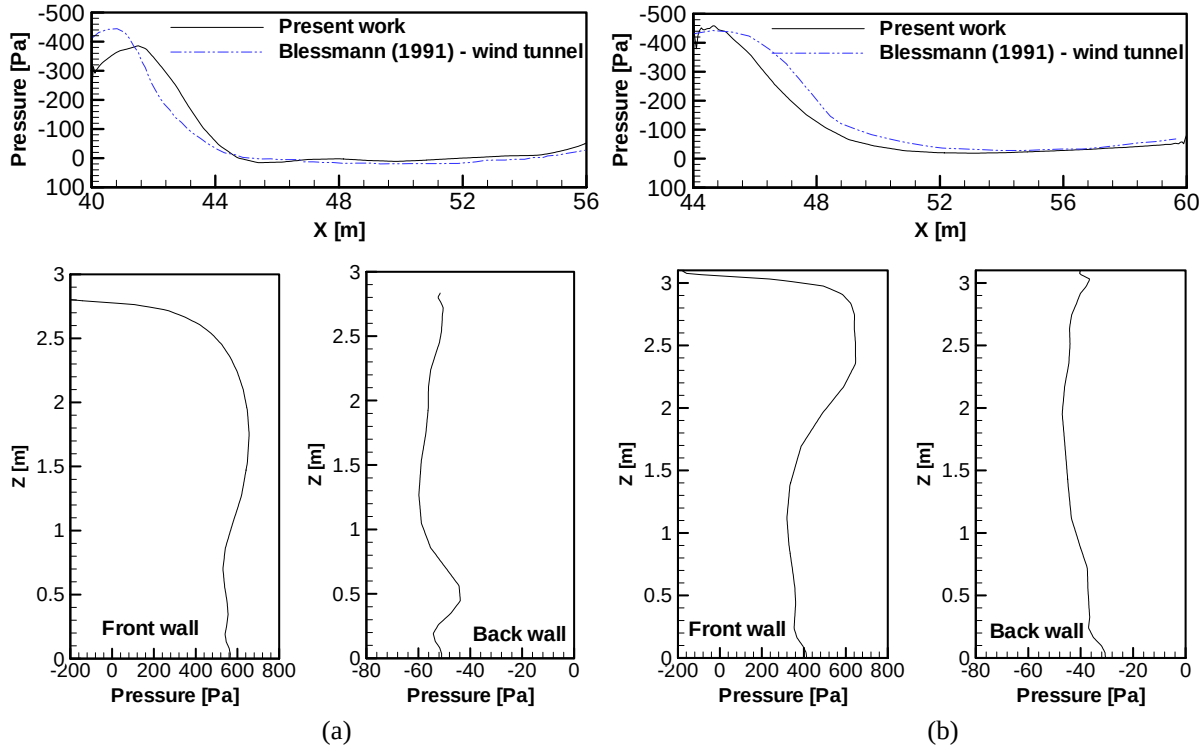

(a) (b)

Figure 5 – Pressure distributions over the intermediate longitudinal sections of the building models: (a) MOD1; (b) MOD 2.

The time average pressure distribution on the lateral walls is presented in Fig. 6 considering a plane referred to the intermediate height of the building models investigated here. Separation can be easily identified observing the high pressure values developed near the separation region. Reattachment is also identified in both cases, since the pressure suction magnitude is significantly reduced for locations far from the separation lines.

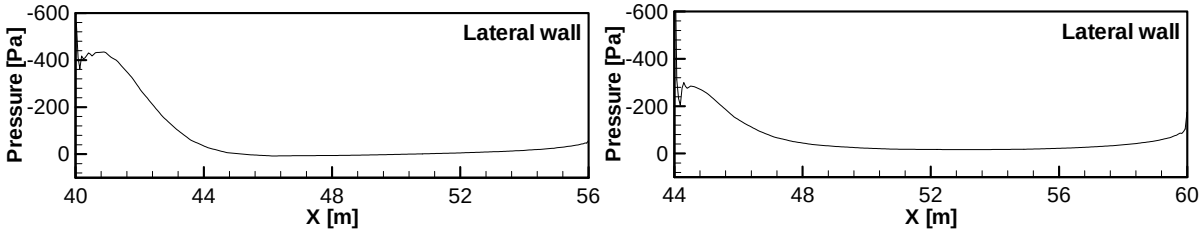

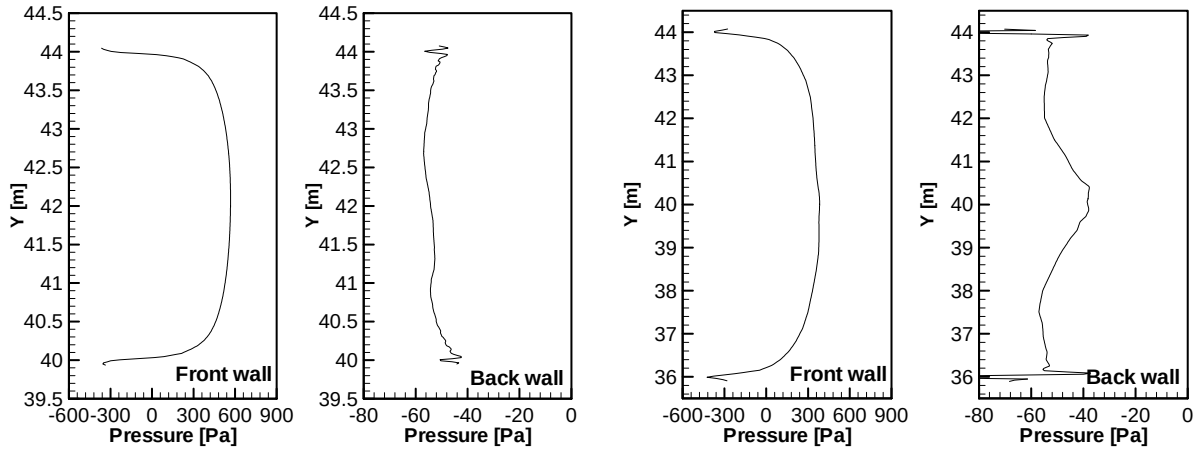

Figure 6 – Pressure distributions over the intermediate vertical sections (h/2) of the building models: (a) MOD1; (b) MOD 2.

In Fig. 7, aerodynamic coefficients referring to drag and lift forces are presented. Time average values can be evaluated considering the time histories obtained from values collected during the numerical simulation by using the evaluation technique explained previously. The results obtained here are in agreement with experimental tests performed by Chien (1951) (see Blessmann, 1991).

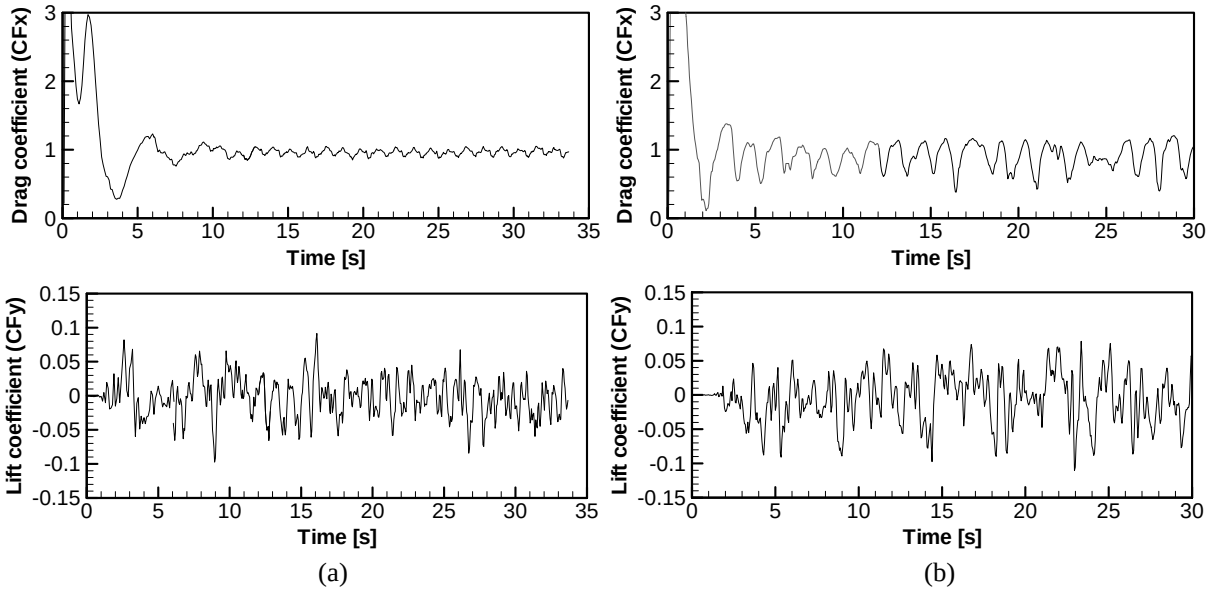

Figure 7 – Aerodynamic coefficents obtained in the present work: (a) MOD1; (b) MOD 2.

The general flow conditions near the building locations can be visualized in Fig. 8, where time average pressure and streamline fields are presented. One can notice that zones with high pressure are developed in the frontal area of the building models owing to the development of horseshoe vortices near the ground. It is also observed that some other important characteristics of the flow field around low-rise buildings were reproduced by the present simulation, such as the development of stagnation zones on the front walls, flow separation along the front corners, reattachment on the roof and lateral walls and recirculation zones behind the building models. These predictions are in accordance with experimental

observations made by Peterka et al. (1985), where detailed information about flow circulation around buildings are presented.

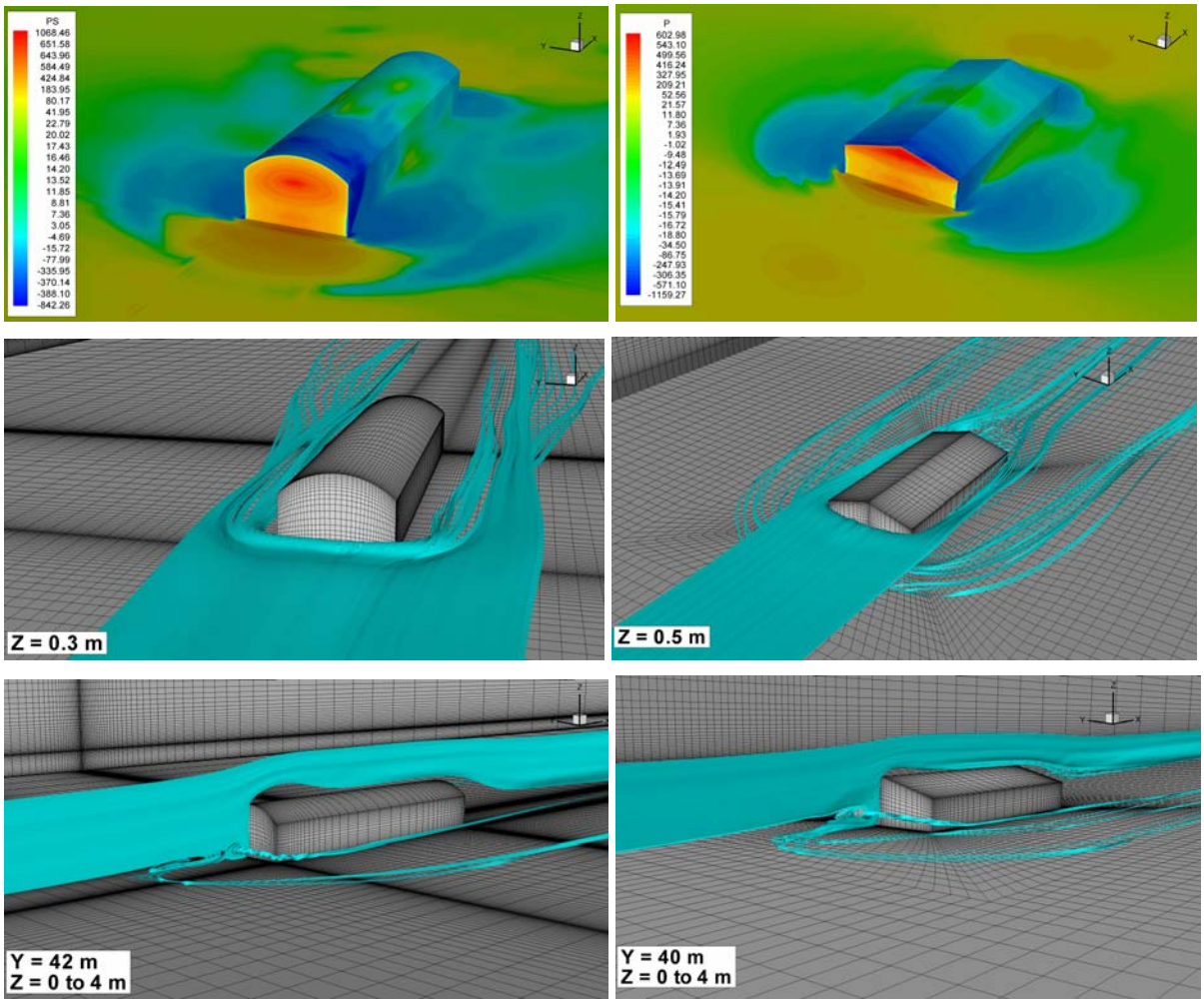

(a) (b)

Figure 8 – Time average fields corresponding to pressure and streamlines: (a) MOD1; (b) MOD 2.

5.2 Aerodynamic analysis of a silo model

In the present application the aerodynamic behavior of a storage silo submitted to atmospheric boundary layer flow is numerically investigated using the numerical model proposed in this work. The silo model is composed of a circular cylindrical shell with a conical roof presenting a roof pitch of 11º. Physical and geometrical constants adopted in the silo analysis are found in Table 3, which are in accordance with the experimental analyses carried out by Portela and Godoy (2005). A Reynolds number Re = 3.0×10^5 is adopted for the flow characterization considering the silo diameter and the streamwise flow velocity at the reference level, which is referred to the height of the cylindrical wall of the silo. In order to reproduce flow characteristics similar to the atmospheric boundary layer on the incident flow, a streamwise velocity profile is defined on the inlet plane considering the power law equation, that is:

$$V_i = V_{\text{ref}} \left(\frac{x_3}{x_3^{\text{ref}}} \right)^p ; \qquad \text{with:} \begin{cases} V_{\text{ref}} = 54 \text{ m/s} \\ x_3^{\text{ref}} = 12 \text{ m} \\ p = 0.15 \end{cases} \tag{22}$$

where V_{ref} and x_{ref} are reference values for velocity and height and p is a constant usually defined according to roughness characteristics of the ground where the structure is located (see Simiu and Scanlan, 1996). In addition, a turbulence intensity of 15% is imposed on the inflow velocity field considering a length scale proportional to the silo diameter.

In Fig. 9 the mesh configuration near the silo location is shown, where the main geometrical parameters are also indicated. The finite element mesh is constituted by 507700 hexahedral elements and 526324 nodal points. Nonslip boundary conditions are considered on the silo surface as well as on the ground level. Outflow boundary conditions with constant pressure distribution and flow symmetry on the side and top walls of the computational domain are also prescribed. The inflow boundary conditions are imposed considering the velocity profile defined by Eq. (22), over which a fluctuating signal is introduced employing the turbulence generator proposed in this work.

Proprieties	
Mass density (ρ) [Kg/m^3]	1.25
Dynamic viscosity (μ) [Ns/m^2]	5.5x10^{-3}
Volumetric viscosity (λ) [Ns/m^2]	0.0
Sound speed (c) [m/s]	250
Reference velocity V_∞ [m/s]	54
Reference dimension D [m]	30.49
Time step Δt [s]	2x10^{-4}

Table 3 – Physical and time constants adopted in the numerical analysis of the silo model.

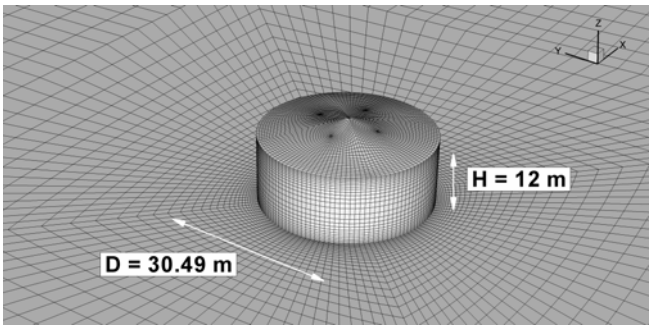

Figure 9 – Finite element mesh utilized in the silo analysis.

The time average pressure distribution over the roof surface is presented in Fig. 10, where predictions obtained in the present analysis are compared with experimental results obtained by Portela and Godoy (2005). Results are presented here in terms of pressure coefficient, which is defined according to Eq. (21) and the respective reference values given by Table 3. A good agreement can be observed with respect to pressure distribution and comparisons between numerical and experimental values of pressure coefficients in different regions of the roof surface show a good agreement as well.

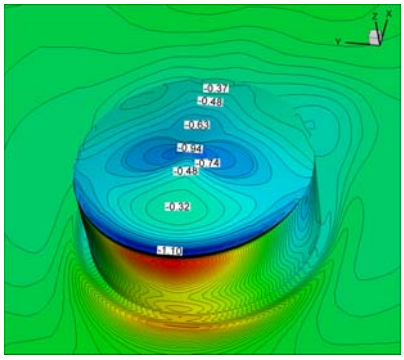

Present work

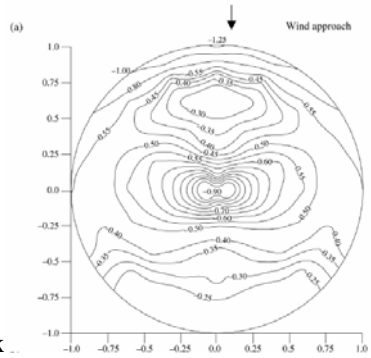

Portela and Godoy (2005)

Figure 10 – Numerical and experimental results related to time average pressure distribution over the roof surface of the silo model.

In order to observe the pressure distribution over the cylindrical shell of the silo model, pressure contour lines are presented in Fig. 11, which are referred to the average pressure field obtained from the present numerical simulation. Three views are presented corresponding to front, lateral and back regions of the cylindrical wall, respectively. In addition, the distribution of the pressure coefficient over the silo perimeter is also shown in the same figure, where simulations with different conditions referring to turbulence intensity are compared. The configurations obtained here follow approximately the same distribution observed in the experimental results presented by authors such as Sabransky and Melbourne (1987), Macdonald et al. (1988) and Portela and Godoy (2005). However, a better agreement is only observed in the front and back regions of the cylindrical wall. Lateral regions of the cylindrical shell present some disagreements with respect to values and pressure distribution, which are more evident for zones close to the respective suction peaks. These disagreements may be associated to differences verified between the experimental and numerical representation of the flow field along the height of the cylindrical wall. Therefore, further investigations are needed in this case.

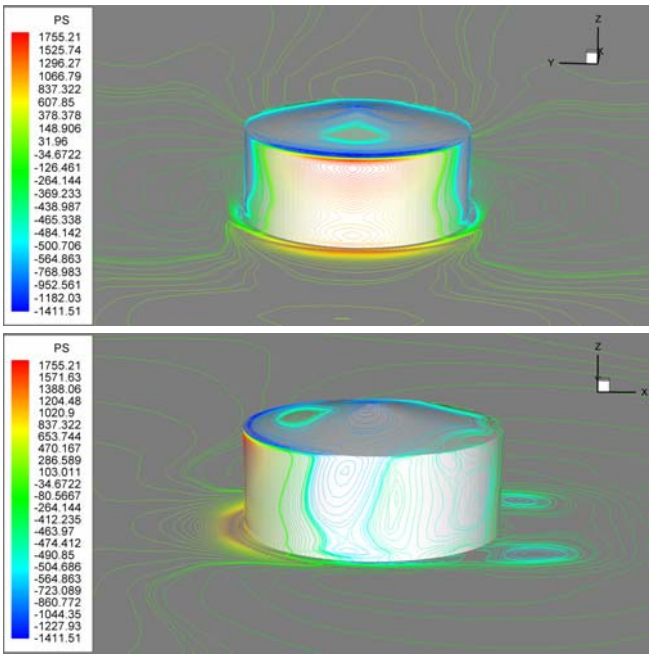

(continue)

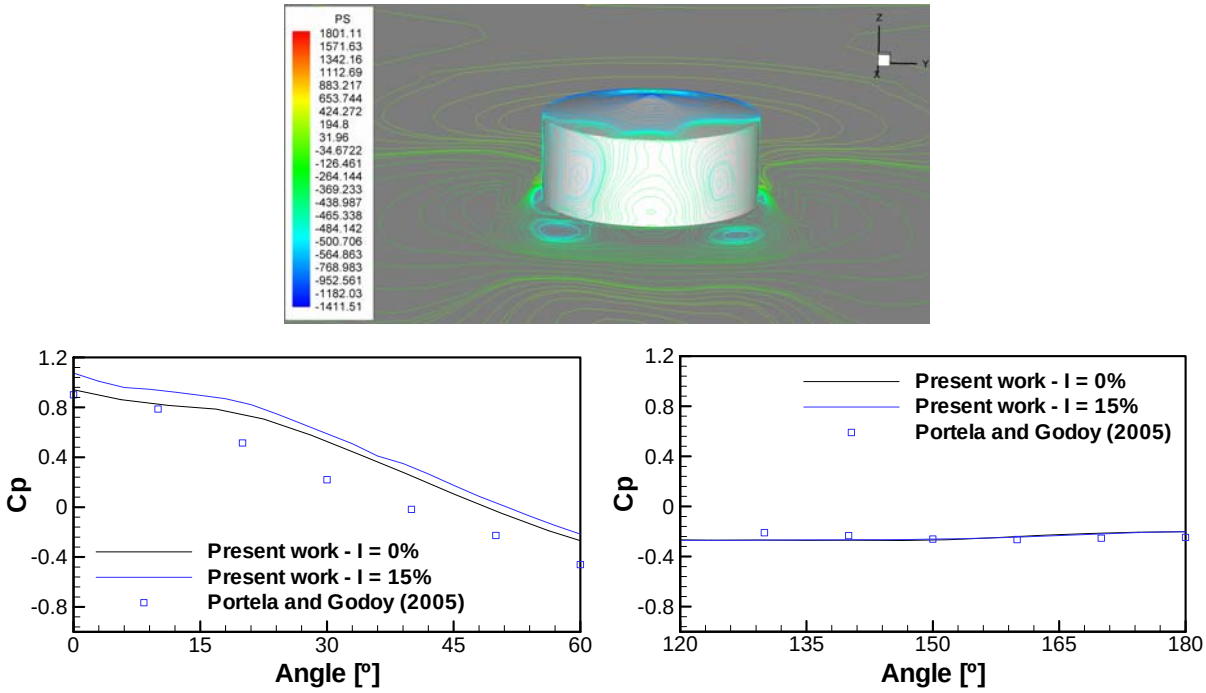

Figure 11 – Pressure isolines and pressure coefficient distributions obtained over the cylindrical wall of the silo model.

In Fig. 12, instantaneous streamlines around the silo model analyzed in this work are presented. Important flow characteristics can be visualized here, such as the horseshoe vortices acting upstream of the silo position and the recirculation regions observed behind and in front of the silo model.

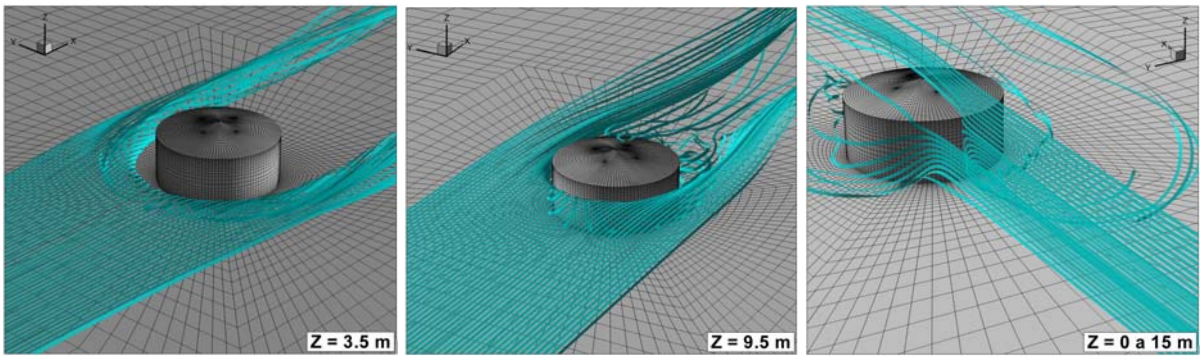

Figure 12 – Instantaneous streamlines obtained in the numerical analysis of the silo model.

6 CONCLUSIONS

A numerical model for investigations on low-rise building aerodynamics was presented in this work. A finite element model based on the explicit two-step Talor-Galerkin scheme was formulated using eight-node hexahedral elements with one-point quadrature. The turbulent flows investigated here were analyzed using LES and the dynamic sub-grid model, where a synthesized turbulence generator was also considered for imposition of fluctuating inflow boundary conditions. Some typical applications were analyzed involving low-rise buildings such as houses and silo models and results obtained by the present numerical model were compared with experimental data from wind tunnel studies. It was verified that the numerical scheme proposed in this paper reproduced well most of the physical phenomena referred to

the examples simulated. Insufficient results are likely associated to deficiencies in the boundary layer representation and spatial discretization. Additional investigations related to the imposition of inflow boundary conditions and mesh discretization will be performed in order to obtain better approximations to the experimental predictions, especially for the silo analysis where simulations with uniform flows will be carried out. In future works, an algorithm for adaptive mesh refinement will be implemented in the present formulation in order to obtain a more efficient model with respect to spatial discretization procedures.

AKNOWLEDGMENTS

The authors would like to thank CNPq (Brazilian Council of Research) for the financial support provided during the present research.

REFERENCES

ABNT – Associação Brasileira de Normas Técnicas, *Forças Devidas ao Vento em Edificações*. NBR 6123. Rio de Janeiro (RJ), 1988.

Blessmann, J. *Ação do Vento em Telhados*, 1ª Edição. Sagra: Porto Alegre, 1991.

Braun, A.L., Simulação Numérica na Engenharia do Vento Incluindo Efeitos de Interação Fluido-Estrutura. D.Sc. Thesis, PPGEC/UFRGS, Porto Alegre (RS), Brasil, 2007.

Braun, A.L. and Awruch, A.M., Aerodynamic and aeroelastic analysis of bundled cables by numerical simulation. *Journal of Sound and Vibration*, 284:51-73, 2005.

Braun, A.L. and Awruch, A.M. Finite element simulation of the wind action over bridge sectional models: application to the Guamá River Bridge (Pará State, Brazil). *Finite Elements in Analysis and Design*, 44:105-122, 2008.

Braun, A.L. and Awruch, A.M., Aerodynamic and aeroelastic analyses on the CAARC standard tall building model using numerical simulation. *Computers and Structures*, 87:564-581, 2009.

CNPTEC/INPE – Centro de Previsão de Tempo e Estudos Climáticos; Instituto Nacional de Pesquisas Espaciais; Ministério da Ciência, Tecnologia e Inovação. *Princípios de Meteorologia e Meio-Ambiente*. Available on http://www.cptec.inpe.br/glossario.shtml.

Chien, N., Feng, Y., Wang, H. and Siao, T. *Wind-Tunnel Studies of Distribution on Elementary Building Forms*. Technical Report, Iowa Institute of Hydraulic Research, Iowa, 1951

Chorin, A.J., A numerical method for solving incompressible viscous flow problems. *Journal of Computational Physics*, 2:12-26, 1967.

Davidson, L. Using isotropic synthetic fluctuations as inlet boundary conditions for unsteady simulations. *Advances and Applications in Fluid Mechanics*, 1:1-35, 2007.

Germano, M., Piomelli, U., Moin, P. and Cabot, W.H., A dynamic subgrid-scale eddy viscosity model. *Physics of Fluids*, A3:1760-1765, 1991.

Huang, S.H., Li, Q.S. and Wu, J.R. A general inflow turbulence generator for large eddy simulation. *Journal of Wind Engineering and Industrial Aerodynamics*, 98:600-617, 2010.

Kawahara, M. and Hirano, H., A finite element method for high Reynolds number viscous fluid flow using two step explicit scheme. *International Journal for Numerical Methods in Fluids*, 3:137-163, 1983.

Klein, M.A., Sadkiki and Janicka, J. A digital filter based generation of inflow data for spatially developing direct numerical or large eddy simulations. *Journal of Computational Physics*, 186:652–665, 2003.

Lilly, D.K., A proposed modification of the Germano subgrid-scale closure method. *Physics of Fluids*, A4:633-635, 1992.

Macdonald, P.A., Kwok, K.S.C. and Holmes, J.D. Wind loads on circular storage bins, silos and tanks: I. point pressure measurements on isolated structures. *Journal of Wind Engineering and Industrial Aerodynamics*, 31:165-188, 1988.

Peterka, J.A., Meroney, R.N. and Kothari, K.M. Wind flow patterns about buildings. *Journal of Wind Engineering and Industrial Aerodynamics*, 21:21-38, 1985.

Portela, G. and Godoy, L.A. Wind pressures and buckling of cylindrical steel tanks with conical roof. *Journal of Constructional Steel Research*, vol. 61, 2005, pp. 786-807.

Sabransky, I.J. and Melbourne, W.H. Design pressure distribution on circular silos with conical roofs. *Journal of Wind Engineering and Industrial Aerodynamics*, 26:65-84, 1987.

Simiu, E. and Scanlan, R.H. *Wind Effects on Structures*, 2nd Edition. John Wiley & Sons: New York, 1996.

Smagorinsky, J., General circulation experiments with the primitive equations, I, the basic experiment. *Monthly Weather Review*, 91:99-135, 1963.

Tamura, T. Towards practical use of LES in wind engineering. *Journal of Wind Engineering and Industrial Aerodynamics*, 96:1451-1471, 2008.

White, F., *Viscous Fluid Flow*, 3rd ed. Mc Graw-Hill, New York, USA, 2005.

Zienckiewicz, O.C., Taylor, R.L. and Nithiarasu, P. *The Finite Element Method for Fluid Dynamics*, 6th ed. Elsevier Butterworth-Heinemann: Oxford, 2005.